

# Designing of Magnetic MAB Phases for Energy Applications

Chen Shen, Qiang Gao, Nuno M. Fortunato, Harish K. Singh, Ingo Opahle, Oliver  
Gutfleisch, and Hongbin Zhang\*

*Institute of Materials Science, Technical University Darmstadt, Alarich-Weiss-Strasse 2,  
64287 Darmstadt, Germany*

E-mail: hzhang@tmm.tu-darmstadt.de

## Abstract

Based on high-throughput density functional theory calculations, we performed screening for stable magnetic MAB compounds and predicted potential strong magnets for permanent magnet and magnetocaloric applications. The thermodynamical, mechanical, and dynamical stabilities are systematically evaluated, resulting in 21 unreported compounds on the convex hull, and 434 materials being metastable considering convex hull tolerance to be 100 meV/atom. Analysis based on the Hume-Rothery rules revealed that the valence electron concentration and size factor difference are of significant importance in determining the stability, with good correspondence with the local atomic bonding. We found 71 compounds with the absolute value of magnetocrystalline anisotropy energy above  $1.0 \text{ MJ/m}^3$  and 23 compounds with a uniaxial anisotropy greater than  $0.4 \text{ MJ/m}^3$ , which are potential gap magnets. Based on the magnetic deformation proxy, 99 compounds were identified as potential materials with interesting magnetocaloric performance.

# Introduction

The modern industrial and societal demands for advanced functional magnetic materials are growing faster as we are witnessing the global expansion of hybrid-electric vehicles, robotics, wind turbines, and automation, leading to a strong incentive on the green energy revolution.<sup>1,2</sup> Particularly, the efficient harvesting of renewable energy (such as wind energy) and endeavor to reduce the greenhouse effect (mainly through the development of e-mobility and magnetic refrigeration) have intensified the impetus to design resource-efficient magnetic materials with optimal performance, such as permanent magnets and magnetocaloric materials. For instance, one interesting question is to identify the so-called gap magnets,<sup>3</sup> *i.e.*, permanent magnets with their energy density  $(BH)_{\max}$ <sup>4</sup> lying between the widely applied AlNiCo and Ferrites<sup>5</sup> and the high-performance Sm-Co<sup>6</sup> and Nd-Fe-B-based<sup>7</sup> permanent magnets. Potential candidates can be characterized using the dimensionless figure of merit  $\kappa = \sqrt{K_1/(\mu_0 M_S^2)}$ ,<sup>8</sup> providing an effective descriptor for high-throughput screening. Moreover, following the discovery of Gd<sub>5</sub>Si<sub>2</sub>Ge<sub>2</sub><sup>9</sup> and LaFeSi<sub>13</sub><sup>10</sup> with giant magnetocaloric effect (MCE) around room temperature, magnetic refrigeration technology is assumed to be capable of competing with and hopefully surpassing conventional refrigeration in terms of energy efficiency, environmentally friendly and ecological impact in the near future.<sup>11–13</sup> However, most permanent magnets and potential magnetocaloric materials with high performance are based on the intermetallic compounds containing rare-earths (RE), which are resource critical.<sup>14</sup> Therefore, rare-earth-free permanent magnets and MCE materials with enhanced efficiency over a broad temperature range and useful secondary properties, such as mechanical stability, corrosion resistance, shapeability, sustainability, and recyclability, are still desirable.<sup>1,15,16</sup>

The MAB phases with nanolaminated crystal structures exhibit intriguing magnetic properties and mechanical deformation behavior, which have attracted considerable attention recently.<sup>17</sup> Such materials are ternary borides comprising stacked M-B layers (M = transition metal, B = Boron) interleaved by monolayers of A atoms. In this regard, the crystal struc-

tures are quite similar to those of the well-known MAX phases  $M_{n+1}AX_n$  ( $X = C$  and  $N$ ,  $A$  denotes a main group element), which host a unique combination of metallic and ceramic properties.<sup>18</sup> The novel magnetic nanolaminates recently discovered in the MAX phases,<sup>19</sup> are also expected in the MAB phases. Moreover,  $Fe_2AlB_2$  was found to be a promising magnetocaloric material exhibiting an interesting MCE,<sup>20</sup> with the ordering temperature around 300 K confirmed by experimental<sup>21,22</sup> and theoretical studies.<sup>23-25</sup> Ke *et al.*<sup>26</sup> investigated the intrinsic properties of  $Fe_2AlB_2$ , and found a MAE as large as  $-1.34$  MJ/cm<sup>3</sup>, in good agreement with the experiments.<sup>22</sup> Recently,  $Cr_4AlB_4$  with a novel structure of MAB phase has been synthesized consistent with the theoretical calculations.<sup>27</sup> Khazaei *et al.*<sup>28</sup> carried out high-throughput (HTP) calculations on Al-containing non-magnetic MAB phases and predicted 9 stable compounds. More recently, Miao *et al.*<sup>29</sup> reported another HTP screening for Ti-A-B, Zr-A-B, and Hf-A-B and predicted 7 thermodynamically stable compounds. Therefore, an interesting question is whether there exist more stable MAB compounds beyond the above-mentioned cases and whether are they good candidates as potential functional magnetic materials.

In this work, based on HTP density functional theory (DFT) calculations, we systematically studied the stabilities and the magnetic properties of the MAB compounds to identify possible candidates for permanent magnets and magnetocaloric materials. Six experimentally synthesized MAB phases and three non-MAB phases (as competitive phases) are considered (Fig. 1), including  $MAB$ <sup>30</sup> (space group  $Cmcm$ ),  $M_2AB_2$ <sup>31</sup> (space group  $Cmcm$ ),  $M_3A_2B_2$ <sup>32</sup> (space group  $Cmcm$ ),  $M_3AB_4$ <sup>33</sup> (space group  $Immm$ ),  $M_4AB_4$ <sup>27</sup> (space group  $Immm$ ) and  $M_4AB_6$ <sup>34</sup> (space group  $Cmcm$ ); non-MAB phases are  $M_5AB_2$ <sup>35</sup> (space group  $I_4/mcm$ ),  $M_3A_2B_2$ <sup>36</sup> (space group  $P2/m$ ) and  $M_4A_3B_2$ <sup>36</sup> (space group  $P4/mmm$ ). Three non-MAB phases are considered as competitive phases in order to make the prediction of MAB compounds more reliable. Such compounds are flexible in the chemical compositions and have tunable magnetic properties. For example,  $Fe_5SiB_2$  has a  $T_C$  higher than 760 K, a  $M_S$  larger than 1 MA/m, and a MAE more than 0.30 MJ/m<sup>3</sup> at room temperature.<sup>37-41</sup> After

validating all the experimentally known phases, we identified stable and metastable ternary borides based on the systematic evaluation of the thermodynamical, mechanical, and dynamical stabilities. Taking the  $M_2AB_2$ -type compounds as an example, we investigated the effect of magnetic ordering on the thermodynamic stability, followed by a comprehensive analysis of the stability trend following the Hume-Rothery rules and local atomic bonding. The MAE and magnetic deformation proxy are evaluated explicitly, which help to screen for potential permanent magnets and magnetocaloric materials. Our work expands the materials library of rare-earth free permanent magnets and magnetic refrigeration, and thus provides valuable guidance to further theoretical and experimental studies to design advanced magnetic materials in transition metal-based ternary borides for energy applications.<sup>13,16</sup>

## Computational details

The DFT calculations are performed using an in-house developed HTP environment<sup>42,43</sup> to determine the thermodynamical stability for the above mentioned six MAB and three non-MAB phases, as demonstrated in recent studies.<sup>44–46</sup> It is noted that the non-MAB phases are regarded as competitive phases for the MAB phase to obtain the reliable convex hull, which is also applied in designing MAX phases by considering antiperovskites as a competitive phase.<sup>45</sup> Thermodynamical stability is evaluated by considering the formation energy ( $E_f$ ) and the distance to the convex hull with respect to all the relevant competing phases available in the OQMD database.<sup>47</sup> All the calculations are carried out using the Vienna ab initio simulation package (VASP) code.<sup>48,49</sup> The MAE of the predicted stable phases is obtained using the full-potential local-orbital (FPLO)<sup>50</sup> code in the force theorem regime, and the recently proposed magnetic deformation proxy<sup>51</sup> is used to evaluate the MCE. More details of the computational processes can be found in the Supplementary.

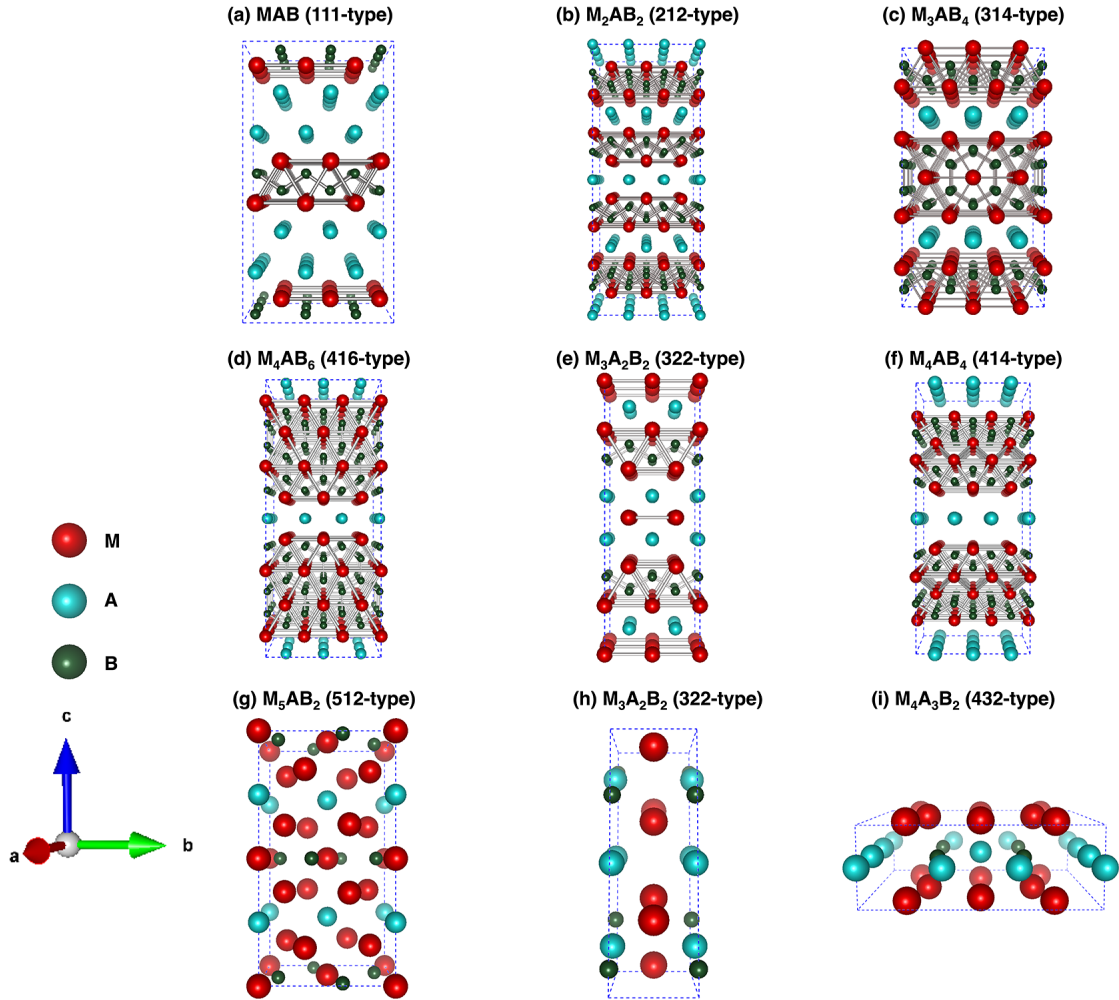


Figure 1: Crystal structures of considered MAB phases(a-f) and non-MAB phases(g-h): (a)222-type [ $Cmcm$ ], (b)212-type [ $Cmcm$ ], (c)314-type [ $Pmmm$ ], (d)416-type [ $Cmmm$ ], (e) 322-type [ $Cmcm$ ], (f) 414-type [ $Immm$ ], (g) 512-type [ $I4/mcm$ ], (h) 322-type [ $P2/m$ ] and (i) 432-type [ $P4/mmm$ ].

# Results and discussion

## Stabilities of phases

### Thermodynamical stability

The thermodynamical stability of the MAB and non-MAB phases (shown in Fig. 1) are obtained based on the formation energy  $\Delta E_f$  and distance to the convex hull  $\Delta E_h$ , where  $\Delta E_f < 0$  and  $\Delta E_h = 0$  are required for the stable phases. In general,  $\Delta E_f < 0$  ensures that the target compounds are energetically stable against decomposing into the constituent elements following the reaction  $M_xA_yB_z \rightarrow xM + yA + zB$ , whereas  $\Delta E_h = 0$  denotes the stability upon the decomposition into any binary and ternary phases according to the reaction  $\Delta E_h = E_{tot}(\text{predicted phase}) - E_{tot}(\text{competing phases})$ . In our calculations, the competing phases include all the relevant compounds found in the OQMD database.<sup>47,52</sup> As summarized in Table. 1, there are 21 compounds satisfying the thermodynamic stability criteria, 17 of them are with one of the MAB structures. According to the literature, 15 ternary borides with one of the considered structures have been experimentally synthesized, as listed in Table. 1. All such compounds exhibit  $\Delta E_f < 0$  and  $\Delta E_h < 80$  meV/atom (due to numerical errors in DFT), validating our methodology and hence the validity of the newly predicted phases. The resulting lattice parameters are in good agreement with the existing measurements and other theoretical calculations, as listed in Table. 1. A special case is  $\text{Co}_5\text{PB}_2$ , where the lattice constants are underestimated (overestimated) along [100] ([001]) directions. This is also observed in previous DFT calculations,<sup>53</sup> which may be driven by the missing spin fluctuations as confirmed in  $(\text{Fe}_{1-x}\text{Co}_x)_2\text{B}$ .<sup>54</sup>

Furthermore, not all the compounds are magnetic, *e.g.*, with finite magnetization larger than  $0.05 \mu_B$  per magnetic atom (Table. 1). It is observed that the nonmagnetic compounds occur mostly for the Cr-, Mn-, and Ni-based cases, whereas  $\text{Fe}_4\text{Al}_3\text{B}_2$  and  $\text{Co}_4\text{Be}_3\text{B}_2$  are nonmagnetic as well. This can be understood based on the Stoner criteria, where  $I\nu(E_F) > 1$  indicate possible itinerant magnetic ordering, with  $I$  being the Stoner parameter and  $\nu(E_F)$

the density of states (DOS) at the Fermi energy  $E_F$  of the nonmagnetic state. For instance, the Stoner parameters of magnetic atoms range between 0.6 and 0.75 from Cr to Ni,<sup>55</sup> thus those compounds with marginal  $\nu(E_F)$  smaller than 1.4 states/eV per magnetic atom end up as nonmagnetic (Fig. S3) because  $I\nu(E_F) < 1$ . Moreover, the predicted results agree well with previous experimental and theoretical reports, *e.g.*,  $\text{Fe}_5\text{PB}_2$  with average magnetization  $1.71 \mu_B/\text{Fe}$ <sup>40</sup> and  $\text{Cr}_4\text{AlB}_{4/6}$  being nonmagnetic.<sup>27,34</sup>

Interestingly, the distance to the convex hull for the experimentally synthesized compounds are finite (Table. 1), *e.g.*,  $\text{Cr}_4\text{AlB}_6$ ,  $\text{Fe}_5\text{PB}_2$  and  $\text{Co}_5\text{PB}_2$  with distances to the convex hull of 12, 33 and 79 meV/atom, respectively. This suggests that a loose tolerance of  $\Delta E_h < 100$  meV/atom is more reasonable, taking into account the temperature effects and the systematic errors in DFT calculations.

Critical tolerance with comparable values for the convex hull has also been adopted in other HTP studies.<sup>43,46,64</sup> This leads to 434 (335 are MAB phases) stable compounds, as listed in Table S1 in the supplementary. As a consequence, our predictions become consistent with another HTP study focusing on Al-containing MAB phases with early transition metals on the M-sites. For instance, 8 novel MAB phases they found, *i.e.*,  $\text{CrAlB}$ ,  $\text{MnAlB}$ ,  $\text{Cr}_3\text{Al}_2\text{B}_2$ ,  $\text{Mn}_3\text{Al}_2\text{B}_2$ ,  $\text{Ni}_3\text{Al}_2\text{B}_2$ ,  $\text{Mn}_3\text{AlB}_4$ , and  $\text{Fe}_3\text{AlB}_4$ , are also predicted to be stable using the loose tolerance on the convex hull, as listed in the Table S1. It is noted that even if such compounds are metastable, they can still be synthesized using non-equilibrium methods such as MBE and ball milling. Hereafter we will consider the stability trend and magnetic properties for all those compounds. Last but not least, it is essential to consider the non-MAB phases as competing phases beyond those in the OQMD database. It is observed that the 322-MAB  $\text{Fe}_3\text{Al}_2\text{B}_2$  is stable with  $\Delta E_h = 0$  compared with competing phases in OQMD, whereas it becomes metastable with  $\Delta E_h = 33$  meV/atom after considering the non-MAB  $\text{Fe}_3\text{Al}_2\text{B}_2$ . Certainly there are other competing phases and even novel crystal structures beyond those considered in this work, which will be saved for future investigation after experimental validations.

Table 1: List of MAB and non-MAB phases that we found stable based on relative stability analysis. The present considered phases experimentally synthesized are indicated by asterisks (\*). Lattice parameters ( $\text{\AA}$ ), formation energy (eV/atom), distance to the convex hull (ev/atom), competing phases, magnetism and magnetic moment ( $\mu B/Mag$ ) in considered phases are shown.

MAB phase	Space group	a	b	c	$\Delta E_f$	$\Delta E_h$	Most competing phases	Magnetism	M
FeBeB	63	2.648	12.164	2.925	-0.326	0	FeB, Be <sub>2</sub> Fe, B	FM	0.422
MnBeB	63	2.811	12.252	2.809	-0.378	0	MnB, Be	NM	0.002
Fe <sub>2</sub> AlB <sub>2</sub> *	65	2.916	11.019	2.851	-0.401	0	FeAl <sub>6</sub> , AlB <sub>2</sub> , FeB	FM	1.330
Ref. Exp. <sup>20</sup>		2.928	11.033	2.868					
Ref. Cal. <sup>26</sup>		2.915	11.017	2.851					
Fe <sub>2</sub> BeB <sub>2</sub>	65	2.904	9.947	2.749	-0.344	0	Be <sub>2</sub> Fe, B, FeB	AFM	0.760
Cr <sub>2</sub> AlB <sub>2</sub> *	65	2.923	11.051	2.932	-0.466	0	Cr <sub>3</sub> AlB <sub>4</sub> , Cr <sub>7</sub> Al <sub>45</sub> , CrB	NM	0.010
Ref. Exp. <sup>34</sup>		2.937	11.051	2.968					
Ref. Cal. <sup>26</sup>		2.921	11.034	2.929					
Mn <sub>2</sub> AlB <sub>2</sub> *	65	2.894	11.080	2.831	-0.471	0	Mn <sub>4</sub> Al <sub>11</sub> , MnB, MnB <sub>4</sub>	AFM	0.765
Ref. Exp. <sup>24</sup>		2.923	11.070	2.899				AFM	
Ref. Cal. <sup>26</sup>		2.887	11.109	2.830				AFM	
Mn <sub>2</sub> BeB <sub>2</sub>	65	2.846	9.969	2.815	-0.435	0	MnB, Be	NM	0.011
Cr <sub>3</sub> AlB <sub>4</sub> *	47	2.939	2.939	8.091	-0.445	0	Cr <sub>2</sub> AlB <sub>2</sub> , CrB <sub>4</sub> , CrB	NM	0.049
Ref. Exp. <sup>34</sup>		2.956	2.978	8.054					
Ref. Cal. <sup>56</sup>		2.938	2.943	8.090					
Cr <sub>4</sub> AlB <sub>6</sub> *	65	2.947	21.328	2.943	-0.422	0.012	CrB <sub>4</sub> , Cr <sub>3</sub> AlB <sub>4</sub> , CrB	NM	0.003
Ref. Exp. <sup>34</sup>		2.952	21.280	3.013					
Ref. Cal. <sup>57</sup>		2.972	21.389	2.961					
Fe <sub>4</sub> AlB <sub>4</sub>	71	2.927	18.565	2.870	-0.417	0	AlFe <sub>2</sub> B <sub>2</sub> , FeB	FM	1.271
Fe <sub>4</sub> BeB <sub>4</sub>	71	2.918	17.513	2.821	-0.377	0	FeB, Be <sub>2</sub> Fe, B	FM	1.017
Fe <sub>4</sub> GaB <sub>4</sub>	71	2.939	18.557	2.883	-0.343	0	FeB, Ga <sub>3</sub> Fe, B	FM	1.288
Fe <sub>4</sub> MgB <sub>4</sub>	71	2.932	19.626	2.875	-0.354	0	FeB, Mg	FM	1.391
Fe <sub>4</sub> ZnB <sub>4</sub>	71	2.931	18.726	2.872	-0.348	0	FeB, Zn	FM	1.326
Cr <sub>4</sub> AlB <sub>4</sub> *	71	2.920	18.856	2.939	-0.510	0	AlCr <sub>2</sub> B <sub>2</sub> , CrB	NM	0
Ref. Exp. <sup>27</sup>		2.934	18.891	2.973					
Ref. Cal. <sup>27</sup>		2.932	18.912	2.957					
Mn <sub>4</sub> BeB <sub>4</sub>	71	2.899	17.591	2.878	-0.467	0	MnB, Be	FM	0.878
Mn <sub>4</sub> AlB <sub>4</sub>	71	2.929	18.591	2.889	-0.499	0	MnB, Mn <sub>2</sub> AlB <sub>2</sub>	FM	1.014
Mn <sub>4</sub> IrB <sub>4</sub>	71	2.959	18.716	2.966	-0.450	0	MnB, Ir	FM	2.003
Ni <sub>4</sub> AuB <sub>4</sub>	71	3.012	18.793	2.950	-0.224	0	Au, Ni <sub>4</sub> B <sub>3</sub> ,	NM	0
Ni <sub>4</sub> CuB <sub>4</sub>	71	2.992	18.125	2.875	-0.227	0	B, Cu, Ni <sub>4</sub> B <sub>3</sub>	NM	0
Ni <sub>4</sub> PdB <sub>4</sub>	71	2.996	18.453	2.931	-0.265	0	Ni <sub>4</sub> B <sub>3</sub> , BPd <sub>2</sub> , B	NM	0
Ni <sub>4</sub> PtB <sub>4</sub>	71	2.995	18.351	2.960	-0.267	0	BPT <sub>2</sub> , Ni <sub>4</sub> B <sub>3</sub> , B	NM	0
Ni <sub>4</sub> ZnB <sub>4</sub>	71	2.992	18.517	2.880	-0.261	0	Ni <sub>4</sub> B <sub>3</sub> , B, ZnNi <sub>3</sub> B <sub>2</sub>	NM	0
Fe <sub>3</sub> Al <sub>2</sub> B <sub>2</sub> *	10	5.685	2.833	8.593	-0.426	0	FeAl <sub>6</sub> , AlB <sub>2</sub> , FeB	FM	0.784
Ref. Exp. <sup>36</sup>		5.723	2.857	2.857					
Fe <sub>3</sub> Al <sub>3</sub> B <sub>2</sub>	123	8.083	8.083	2.791	-0.411	0	AlFe, AlFe <sub>2</sub> B <sub>2</sub>	NM	0.002
Co <sub>4</sub> Be <sub>3</sub> B <sub>2</sub>	123	7.586	7.586	2.586	-0.395	0	Be <sub>3</sub> Co, BeCo, CoB	NM	0
Ni <sub>4</sub> Li <sub>3</sub> B <sub>2</sub>	123	8.049	8.049	2.734	-0.252	0	Li, Ni <sub>2</sub> B	NM	0.0002
Fe <sub>5</sub> BeB <sub>2</sub>	140	5.455	5.455	9.914	-0.292	0	Be <sub>2</sub> Fe, Fe <sub>2</sub> B, Fe	FM	1.932
Fe <sub>5</sub> PB <sub>2</sub> *	140	5.570	5.570	10.436	-0.392	0.033	Fe <sub>2</sub> B, FeB, Fe <sub>2</sub> P	FM	1.705
Ref. Exp. <sup>35</sup>		5.548	5.548	10.332				FM	1.730
Ref. Exp. <sup>38</sup>		5.487	5.487	10.353				FM	1.600
Ref. Exp. <sup>40</sup>		5.485	5.485	10.348				FM	1.720
Ref. Exp. <sup>41</sup>		5.503	5.503	10.347					
Ref. Exp. <sup>58</sup>		5.492	5.492	10.365				FM	1.658
Ref. Cal. <sup>53</sup>		5.456	5.456	10.296				FM	1.770
Fe <sub>5</sub> SiB <sub>2</sub> *	140	5.509	5.509	10.299	-0.359	0.003	Fe <sub>2</sub> B, FeSi	FM	1.731
Ref. Exp. <sup>38</sup>		5.551	5.551	10.336				FM	1.808
Ref. Exp. <sup>37</sup>		5.554	5.554	10.343				FM	1.750
Ref. Cal. <sup>39</sup>		5.546	5.546	10.341				FM	1.840
Co <sub>5</sub> PB <sub>2</sub> *	140	5.279	5.279	10.477	-0.357	0.079	Co <sub>2</sub> P, CoB, Co	FM	0.409
Ref. Exp. <sup>59</sup>		5.420	5.420	10.200					
Ref. Cal. <sup>53</sup>		5.284	5.284	10.541				FM	0.440
Co <sub>5</sub> SiB <sub>2</sub> *	140	5.484	5.484	9.942	-0.337	0.042	CoB, Co <sub>2</sub> Si, Co	FM	0.394
Ref. Exp. <sup>60</sup>		5.511	5.511	9.953				FM	0.484
Ref. Cal. <sup>39</sup>		5.537	5.537	10.317	-0.474	0.032	Cr <sub>3</sub> P, CrB	NM	0.022
Cr <sub>5</sub> PB <sub>2</sub> *	140	5.537	5.537	10.317	-0.474	0.032	Cr <sub>3</sub> P, CrB	NM	0.022
Ref. Exp. <sup>61</sup>		5.593	5.593	10.370					
Cr <sub>5</sub> B <sub>4</sub> *	140	5.431	5.431	9.923	-0.418	0	CrB, Cr <sub>2</sub> B	NM	0
Ref. Exp. <sup>62</sup>		5.460	5.460	10.460					
Mn <sub>5</sub> PB <sub>2</sub> *	140	5.509	5.509	10.287	-0.480	0.033	Mn <sub>2</sub> B, MnB, Mn <sub>2</sub> P	FM	1.665
Ref. Exp. <sup>59</sup>		5.540	5.540	10.490					
Ref. Exp. <sup>63</sup>		5.540	5.540	10.490					
Mn <sub>5</sub> SiB <sub>2</sub> *	140	5.559	5.559	10.293	-0.415	0.003	MnSi, Mn <sub>2</sub> B	FM	1.583
Ref. Exp. <sup>63</sup>		5.540	5.540	10.490					

Another interesting question for predicting stable magnetic materials is whether the magnetic configurations would influence the thermodynamic stability, since most HTP calculations are done assuming the ferromagnetic (FM) state as in the OQMD and the Materials Project.<sup>65</sup> This applies particularly to Mn-based compounds, as revealed by a recent work that the energy landscape of the convex hull is drastically changed after considering the magnetic ground state.<sup>66</sup> According to the literature, the 212-type  $\text{Mn}_2\text{AlB}_2$  is observed to display an AFM magnetic ground state with Néel temperature about 390 K,<sup>26,67,68</sup> thus we performed extensive calculations on the predicted 212-type MAB compounds. As summarized in Table.S2, 15 out of 54 magnetic compounds prefer AFM magnetic configurations, including not only Mn-based but also Fe- and Co-based compounds. The magnetic ground states are consistent with those obtained from our Monte Carlo modeling based on the Heisenberg model taking exchange parameters from DFT calculations (not shown), which will be discussed in detail elsewhere. Nevertheless, the energy difference between the FM and AFM states is less than 20 meV per atom, hence the magnetic ground state has no strong impact on the thermodynamic stability for such compounds. This can be attributed to the nano-laminated crystal structure, where the magnetic interaction between the local Mn-moments is relatively weak, in comparison to the strongly frustrated fcc-lattice from the  $\text{Cu}_3\text{Au}$  lattice considered in Ref.<sup>66</sup> It is noted that systematic evaluation of the magnetic ground states is a challenge, hereafter we will focus on the physical properties of the FM states, which should be valid for most of the other compounds.

After the thermodynamic stability, mechanical and dynamical stabilities should be addressed as well in order to make systematic predictions. It is observed that mechanical stability plays a marginal role as explicitly demonstrated for 21 stable compounds on the convex hull. This is consistent with our previous studies on the antiperovskite compounds.<sup>46</sup> For the orthorhombic MAB phases, there are nine independent elastic constants  $C_{11}$ ,  $C_{22}$ ,  $C_{33}$ ,  $C_{44}$ ,  $C_{55}$ ,  $C_{66}$ ,  $C_{12}$ ,  $C_{13}$ , and  $C_{23}$ . For the tetragonal non-MAB phases, there are six independent elastic constants  $C_{11}$ ,  $C_{33}$ ,  $C_{44}$ ,  $C_{66}$ ,  $C_{12}$ , and  $C_{13}$ . According to the mechanical

stability defined in the Ref.,<sup>69</sup> none of the novel compounds predicted to be thermodynamically stable is found to be mechanically unstable. In addition, the dynamical stability is verified by examining the the phonon spectra as compiled in Fig. S2 for 21 predicted and 15 known cases. Obviously, there is no imaginary modes observed for 35 compounds, indicating that those compounds are stable against local atomic displacements. The resulting phonon spectra for  $\text{Cr}_2\text{AlB}_2$  and  $\text{Cr}_3\text{AlB}_4$  are in good agreement with previous reported results.<sup>70</sup>

Nevertheless, for  $\text{Ni}_4\text{Li}_3\text{B}_2$  there exists an imaginary mode at the M point. This suggests that the compound may end up with other crystal structures or synthesized on certain substrates using molecular beam epitaxy.

### Trends in the stability

To understand the trend of stabilities for the MAB and non-MAB phases, the number of stable compounds ( $\Delta E_h < 100$  meV/atom) with respect to the **A** element are shown in Fig. S4. It is obvious that most elements in the periodic table act as a constituent element stabilizing at least one of the considered crystal structures, whereas nine out of 59 elements (*i.e.*, K, Rb, Cs, Sr, Ba, Zr, N, Sb, and Bi) do not form any stable phases. Particularly, each of the five elements like Be, Al, Pt, Zn, and Ir support more than 22 stable phases. Moreover, among all the structure types considered in this work, 136 compounds are stable with the 414-type structure, albeit the first compound  $\text{Cr}_4\text{AlB}_4$  was reported in 2019.<sup>27</sup>

Taking the 212-type MAB structure as an example, the stability trend with respect to the chemical composition can be understood based on the Hume-Rothery rules.<sup>71</sup> Such rules are formulated based on the difference of size, electronegativity factors and the valence electron concentration (VEC). It is observed that the electronegativity difference between the M and A elements has no strong correlation with the stability (Fig. S5), same as the MAX compounds.<sup>72</sup> On the other hand, as shown in Fig. 2, both the atomic radius difference of the M and A elements  $\frac{|R_M - R_A|}{R_A}$  and VEC have significant influence on the stability. Clearly, most stable compounds are within the region  $\frac{|R_M - R_A|}{R_A} < 0.4$  and  $\text{VEC} < 5.5$ . The newly



to 8 in  $\text{Fe}_2\text{AlB}_2$ , and finally to 10 in  $\text{Ni}_2\text{AlB}_2$ . For  $\text{Cr}_2\text{AlB}_2$ , it is obvious that the values of -COHP are all positive below the Fermi energy, indicating only bonding states are occupied in the corresponding bonds, which leads to a high overall stability (Fig. S8). Increasing the number of valence electron to 10 in  $\text{Ni}_2\text{AlB}_2$ , the negative energies -COHP appeared below the Fermi energy in the Ni-B, Ni-Al, and Ni-Ni bonds. The occupation of such anti-bonding states weakens the bonds and therefore destabilizes the  $\text{Ni}_2\text{AlB}_2$  compound. Therefore, the ICOHP of M-Al and M-B are increasing within the the number of valence electron increasing, which indicates the corresponding bond strength weakens. Similar behaviour is also observed in the COHP os  $\text{Fe}_2\text{AB}_2$  compounds with varying A elements being Be, Ca, and Ba (Fig. S8). As the atomic size changes from 0.99 (Be), 1.74 (Ca) and 2.06 (Ba), the bond strength of those compounds becomes weaker, which are confirmed by the COHP values of Fe-Fe, Fe-B, Fe-A and A-B.

Hence, with respect to varying both M and A elements with increasing number of valence electrons and atomic size, the Fermi energy is shifted into the anti-bonding states, leading to instability. This helps to understand the trend observed in Fig. 2, which provide valuable guidance to guide the synthesis of MAB phases by substituting the M/A sites or via forming solid solutions.

## Magnetic properties

### MAE

Turning now to the magnetic properties, we focus on the magnetocrystalline anisotropy energy (MAE) and magnetocaloric effect (MCE), in order to identify potential candidates for permanent magnet and magnetocaloric applications. The MAE is caused by the broken continuous symmetry of magnetization directions due to the spin-orbit coupling (SOC),<sup>74</sup> which is defined (denoted as K) in terms of

$$K_{\hat{n}_1-\hat{n}_2} = E_{\hat{n}_1} - E_{\hat{n}_2}, \tag{1}$$

where  $E_{\hat{n}}$  denotes the total energy with the magnetization direction parallel to  $\hat{n}$ . In the present work, we consider  $\hat{n}$  along three crystalline directions, namely, [100], [010] and [001], as MAB compounds have orthorhombic structures (Fig. 1). This leads to three MAEs, *i.e.*,  $K_{001-010}$ ,  $K_{001-100}$  and  $K_{010-100}$ . Fig. 3 shows the MAE with respect to the saturation magnetization ( $M_S$ ), in comparison with the experimentally known permanent magnets. There are in total 71 cases (cf. Table. S6 in the supplementary) with the absolute value of at least one MAE greater than  $1.0 \text{ MJ/m}^3$ . For instance, the MAE of  $\text{Fe}_2\text{AlB}_2$  has been evaluated by different groups,<sup>21,22,26</sup> and our result of  $-1.14 \text{ MJ/m}^3$  is in good agreement with the experimental measurements of  $-0.9 \text{ MJ/m}^3$  at 50 K by Barua<sup>22</sup> and theoretical calculation  $-1.34 \text{ MJ/m}^3$  by Ke.<sup>26</sup> In the newly predicted compounds, the MAB phase  $\text{Mn}_4\text{PtB}_4$  has the largest MAE as 13.498, 11.948 and  $-1.550 \text{ MJ/m}^3$  for  $K_{001-010}$ ,  $K_{001-100}$  and  $K_{010-100}$ . Additionally, the 111-type  $\text{FePtB}$  shows the largest MAE in non-Mn-containing compounds as  $-10.646$ , 7.225 and  $-3.421 \text{ MJ/m}^3$  for  $K_{010-100}$ ,  $K_{001-010}$  and  $K_{001-100}$ , suggesting the *b*-direction (*c*-direction) is easy (hard) axis. Based on the dimensionless figure of merit  $\kappa = \sqrt{K_1/(\mu_0 M_S^2)}$ ,<sup>8</sup> there exist quite a few compounds which can be classified as hard magnets. Particularly, the MAE of such ternary TM borides fill the gap between the widely used low performance magnets (such as  $\text{AlNiCo}$  and ferrite) and high performance magnets (such as  $\text{Sm-Co}$  and  $\text{Nd-Fe-B}$ ).

However, not only the absolute values of the MAE but also the sign matters, *e.g.*, the easy axis (direction with the lowest energy) is ideally aligned along a special crystalline axis. For all the MAB compounds, the [001] direction along the stacking direction of the M-B layers (Fig. 1) is chosen, corresponding to the most-probably exposed surfaces for such nano-laminated structures. For the non-MAB phases of the tetragonal space groups, the special axis is chosen to be the axis of 4-fold rotational symmetry, *i.e.*, the [001] direction in Fig. 1(g & i). The MAE for the 322-type compounds (Fig. 1(h)) is overall small thus we do not consider them. Correspondingly, we found 16 MAB and 7 non-MAB phases with a significant out-of-plane MAE ( $> 0.4 \text{ MJ/m}^3$ ), as well as 33 (18) MAB (non-MAB)

compounds with a reasonable in-plane MAE (absolute value larger than  $0.4 \text{ MJ/m}^3$ ), as listed in Table S7. Among them, the 322-type MAB compound  $\text{Mn}_3\text{Ir}_2\text{B}_2$  has the largest out-of-plane MAE of  $10.17 \text{ MJ/m}^3$  for  $K_{010-001}$ , and  $\text{Fe}_2\text{ReB}_2$  with a large MAE of  $9.00 \text{ MJ/m}^3$  in  $K_{010-001}$ . Interestingly, the MAE value of  $\text{Fe}_3\text{Zn}_2\text{B}_2$  is as large as  $3.00 \text{ MJ/m}^3$  in  $K_{100-001}$  while its  $M_s$  is comparable to that of  $\text{MnAl}$ . It contains no expensive, toxic or critical element, which is a good candidate permanent magnet material. Moreover,  $\text{Fe}_7\text{B}_2$  has a sizable MAE  $0.681 \text{ MJ/m}^3$ , which is quite comparable to that of hcp Co. Such a phase is beyond the known binary Fe-B phase diagram,<sup>75</sup> which might be synthesizable under non-equilibrium conditions. Last but not least, the diagram (Fig. 3) together with Table S6 give us a chart to engineer permanent magnets via doping. For instance, our calculations reveal

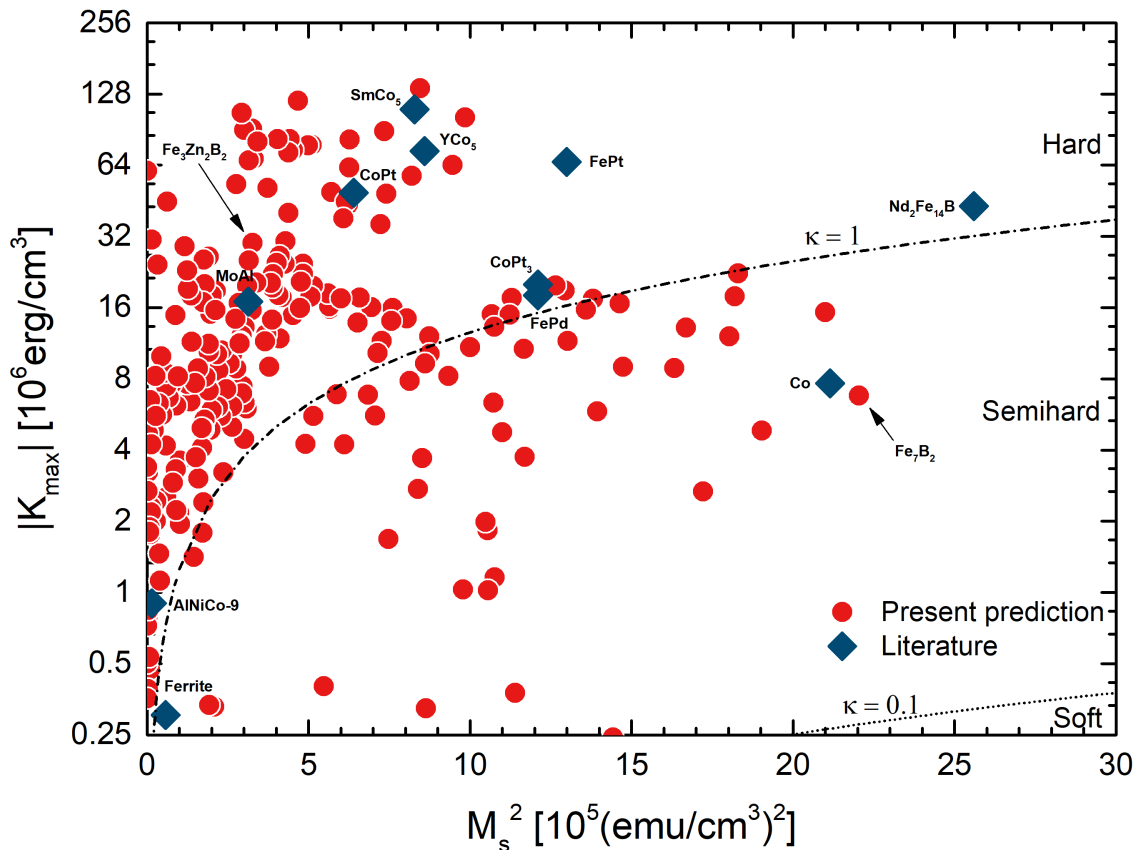


Figure 3: The MAE vs magnetization of the promising candidates of targeted phases. The dashed lines correspond to magnetic hardness parameter  $\kappa = \sqrt{K_1/(\mu_0 M_s^2)}$  for values  $\kappa = 1$  and  $0.1$ . Hard magnetic materials ( $\kappa > 1$ ) can be used to make efficient permanent magnets of any shape.

that  $\text{Fe}_5\text{PB}_2$  has an MAE of  $0.63 \text{ MJ/m}^3$  consistent with the experimental measured value of  $0.65 \text{ MJ/m}^3$ ,<sup>41</sup> whereas a recent work demonstrated that its MAE can be enhanced by substitutionally doping tungsten.<sup>76</sup>

As discussed above, most compounds with significant MAE contain  $5d$  elements, such as Pt, Ir, and Re. This suggests that the MAE is originated from the enhanced atomic SOC strength for the  $5d$ -shell of such elements. Following Ref.,<sup>77</sup> the atomic resolved SOC energy changes are listed in Table. S8 for the 111-type  $\text{FeXB}$  with  $X = \text{Ni, Pd, and Pt}$ . As the atomic SOC strength increases from  $98 \text{ meV}$  for Ni,  $185 \text{ meV}$  for Pd, to  $533 \text{ meV}$  for Pt,<sup>78</sup> the contribution from the X element to the MAE is becoming more significant, as given by the change of atom-resolved SOC energy  $\Delta E_{\text{SOC}} = E_{\text{SOC}}(\hat{n}_1) - E_{\text{SOC}}(\hat{n}_2)$ . For  $\text{FeNiB}$ ,  $\Delta E_{\text{SOC}}(\text{Fe})$  ( $-0.492 \text{ meV/at.}$  in  $[100]$ - $[010]$  direction) dominates the total  $\Delta E_{\text{SOC}}$  ( $-0.586 \text{ meV/f.u.}$  in  $[100]$ - $[010]$  direction) of the compound, as the SOC strength is comparable for Fe ( $55 \text{ meV}$ ) and Ni. Furthermore, for  $\text{FeXB}$  with  $X = \text{Ni, Pd, and Pt}$ , the  $\Delta E_{\text{SOC}}$  of Ni, Pd, and Pt are  $-0.093$ ,  $0.702$ , and  $2.603 \text{ meV/atom}$  between two magnetization directions  $[100]$  and  $[010]$ , corresponding to the changes in the total MAE of  $-0.128$ ,  $0.181$ , and  $2.106 \text{ meV/atom}$ , respectively. That is,  $\Delta E_{\text{SOC}}$  of X has a more dominant contribution to the total  $\Delta E_{\text{SOC}}$  and hence the MAE, when moving down the group from  $3d$  to  $5d$  elements. In the  $\text{FePtB}$ , the contribution of  $\Delta E_{\text{SOC}}$  of Pt is  $84\%$  in total  $\Delta E_{\text{SOC}}$ . Therefore, like  $\text{FePt}$ ,<sup>79</sup> the  $5d$  elements have a more significant contribution to the MAE because of enhanced atomic SOC strength, though the magnetic moments on such elements are induced by those of the  $3d$  atoms.

## MCE

As introduced above, it is postulated that ternary TM borides are promising candidates for MCE applications, such as  $\text{Fe}_5\text{SiB}_2$ <sup>37</sup> and  $\text{Fe}_2\text{AlB}_2$ .<sup>20-22,25</sup> To search for more candidates in the predicted MAB and non-MAB compounds, we performed screening based on the magnetic deformation proxy.<sup>51</sup> It is demonstrated that the magnetic entropy change  $\Delta S_M$

upon magneto-structural transitions has a strong correlation with the magnetic deformation  $\Sigma_M = \frac{1}{3}(\eta_1^2 + \eta_2^2 + \eta_3^2)^{1/2} \times 100$  and  $\boldsymbol{\eta} = \frac{1}{2}(\mathbf{P}^T \mathbf{P} - \mathbf{I})$  where  $\mathbf{P} = \mathbf{A}_{\text{nonmag}}^{-1} \cdot \mathbf{A}_{\text{mag}}$  with  $\mathbf{A}_{\text{nonmag}}$  and  $\mathbf{A}_{\text{mag}}$  being the lattice constants of the nonmagnetic and magnetic unit cells. Although there is no direct scaling between  $\Delta S$  and  $\Sigma_M$ , it is suggested that  $\Sigma_M > 1.5\%$  is a reasonable cutoff to select the promising compounds.<sup>51</sup>

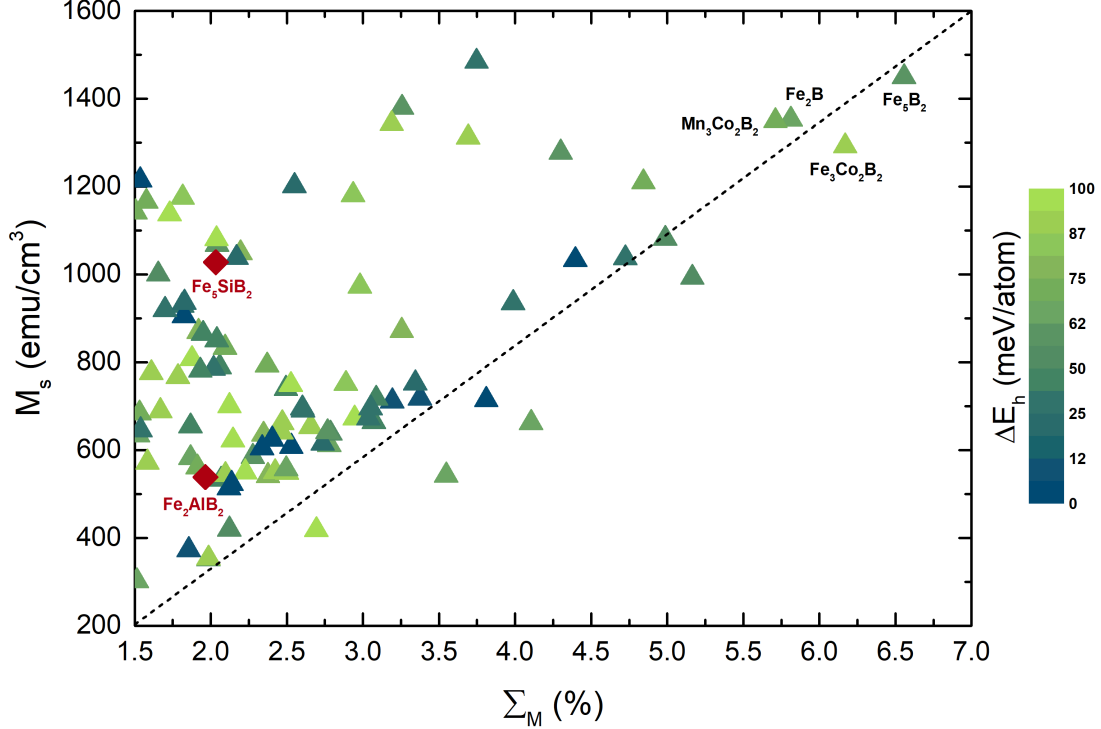


Figure 4: The 99 potential MCMs with magnetic deformation  $\Sigma_M > 1.5\%$ . The color bar marks the distance to the convex hull. The dash line indicates a positive correlation between the magnetization density and the magnitude of magnetic deformation.

Fig. 4 shows the 99 potential MCMs with  $\Sigma_M > 1.5\%$  from 434 compounds with convex hull  $\Delta E < 100$  meV/atom. Among them, the reported<sup>51</sup>  $\Sigma_M$  of  $\text{Fe}_5\text{SiB}_2$  (2.14%) and  $\text{Fe}_2\text{AlB}_2$  (2.05%) are confirmed in our calculations, with the resulting  $\Sigma_M$  of 2.03 % and 1.96 %, respectively. Interestingly, there is positive correlation between the magnetization density and the magnitude of magnetic deformation, *i.e.*, as the magnetic deformation increases, the magnetization of compounds also increase (Fig. 4). It is noted that 82 out of 99 potential MCMs locating at  $\Sigma_M < 3.5\%$ , and the magnetization concentrating between 500

to 1000 emu/cm<sup>3</sup>. Particularly, there are four compounds, *e.g.*, Fe<sub>5</sub>B<sub>2</sub> (322-MAB), Fe<sub>3</sub>Co<sub>2</sub>B<sub>2</sub> (322-MAB), Mn<sub>3</sub>Co<sub>2</sub>B<sub>2</sub> (322-MAB), and Fe<sub>2</sub>B (111-MAB), at the upper-right corner, which perform on both large magnetization and magnetic deformation. We suspect such compounds can exhibit significant  $\Delta S_M$  upon second order phase transition at the corresponding Curie temperature, which will be saved for detailed investigation in the future.

Several important aspects on possible MCE in such materials are noteworthy, based on the distributing map with respect to the **M** and **A** sites as shown in Fig. S9. For instance, compounds with Fe and Mn occupying the **M**-site show a high possibility to possess a large MCE based on the magnetic deformation, which have been confirmed in several reported compounds.<sup>63,80,81</sup> Based on the correlations observed in known MCMs in Ref.,<sup>51</sup> such materials are likely to show a strong magnetocaloric effect and are therefore excellent candidates for experimental study. Moreover, compounds with Mn/Fe/Co, Ru/Rh/Pd and Os/Ir/Pt occupying the **A**-site also show a high potential to host remarkable magnetocaloric properties. Furthermore, it is noted the fact that Fe<sub>2</sub>AlB<sub>2</sub> is composed entirely of earth-abundant elements. This provides a major advantage at least from a cost and resource point of view, over the competing MCMs that contain expensive critical elements (*e.g.*, Gd, Gd<sub>5</sub>Si<sub>2</sub>Ge<sub>2</sub>, FeRh). Therefore, such economic material without critical elements appears especially appealing to us, and the present system M<sub>x</sub>A<sub>y</sub>B<sub>z</sub>, when A = Al, Zn, Si and Fe should be attracted more attention, such as Fe<sub>4</sub>AlB<sub>4</sub> (2.33 %), Fe<sub>3</sub>AlB<sub>4</sub> (2.11 %), Fe<sub>4</sub>SiB<sub>4</sub> (2.73 %), Fe<sub>3</sub>ZnB<sub>4</sub> (2.42 %) and Fe<sub>5</sub>B<sub>2</sub> (*Cmmm*, 6.56 %) (Fig. S9).

## Conclusion

In summary, our high-throughput screening on 6 types of MAB phases and 3 types of competing non-MAB phases predict 434 magnetic ternary transition metal borides which are potential candidates for permanent magnets and magnetocaloric materials. After validating the 15 reported compounds, 21 novel compounds are identified to be stable based on

the systematic evaluation of thermodynamic, mechanical, and dynamical stabilities, and the number of stable compounds is increased to 434 taking the tolerance of convex hull being 100 meV/atom. It is observed that the magnetic ground state for such compounds with layered structures does not have a strong influence on the thermodynamic stability. The trend of stability for the MAB phase can be understood based on the Hume-Rothery rules, where the size factor difference and the valence electron concentration play a critical role. Such a trend can be further attributed to the bond-resolved COHP, providing intuitive guidance for experimental synthesis. The detailed evaluation of the magnetocrystalline anisotropy energy and the magnetic deformations leads to 23 compounds with significant uniaxial anisotropy ( $> 0.4 \text{ MJ/m}^3$ ) and 99 systems with reasonable magnetic deformation ( $\sum_M > 1.5\%$ ). For those compounds containing no expensive, toxic, or critical elements, it is observed that  $\text{Fe}_3\text{Zn}_2\text{B}_2$  is a reasonable candidate as gap permanent magnet, and  $\text{Fe}_4\text{AlB}_4$ ,  $\text{Fe}_3\text{AlB}_4$ ,  $\text{Fe}_3\text{ZnB}_4$ , and  $\text{Fe}_5\text{B}_2$  as potential magnetocaloric materials. This work paves the way for designing more magnetic materials for energy applications and magnetic MBene for two-dimensional magnetic materials. At last, the realistic assessment of the predicted potential MAB phases are conducting and will add to our library<sup>13,16</sup> soon.

## Acknowledgement

The authors gratefully thank Manuel Richter for providing the SOC strength data and helpful discussions. This work was also supported by the Deutsche Forschungsgemeinschaft (DFG, German Research Foundation) - Project-ID 405553726 - TRR 270. Part of this work was supported by the European Research Council (ERC) under the European Union's Horizon 2020 research and innovation program (Grant No. 743116-project Cool Innov) The Lichtenberg high performance computer of the TU Darmstadt is gratefully acknowledged for the computational resources where the calculations were conducted for this project.

## Supporting Information Available

The following files are available free of charge. Numerical details, list of all metastable compounds, and additional theoretical results can be found in the Supplementary Material.

## References

- (1) Gutfleisch, O.; Willard, M. A.; Brück, E.; Chen, C. H.; Sankar, S.; Liu, J. P. Magnetic materials and devices for the 21st century: stronger, lighter, and more energy efficient. *Adv. Mater.* **2011**, *23*, 821–842.
- (2) Skokov, K.; Gutfleisch, O. Heavy rare earth free, free rare earth and rare earth free magnets-vision and reality. *Scr. Mater.* **2018**, *154*, 289–294.
- (3) Coey, J. Permanent magnets: Plugging the gap. *Scr. Mater.* **2012**, *67*, 524–529.
- (4) Gutfleisch, O. Controlling the properties of high energy density permanent magnetic materials by different processing routes. *J. Phys. D Appl. Phys.* **2000**, *33*, 157.
- (5) Sugimoto, S. Current status and recent topics of rare-earth permanent magnets. *J. Phys. D Appl. Phys.* **2011**, *44*, 064001.
- (6) Strnat, K. J.; Strnat, R. M. Rare earth-cobalt permanent magnets. *J. Magn. Magn. Mater.* **1991**, *100*, 38–56.
- (7) Herbst, J.; Croat, J. Neodymium-iron-boron permanent magnets. *J. Magn. Magn. Mater.* **1991**, *100*, 57–78.
- (8) Coey, J. New permanent magnets; manganese compounds. *J. Condens. Matter Phys.* **2014**, *26*, 064211.
- (9) Pecharsky, V. K.; Gschneidner Jr, K. A. Giant magnetocaloric effect in  $\text{Gd}_5(\text{Si}_2\text{Ge}_2)$ . *Phys. Rev. Lett.* **1997**, *78*, 4494.

- (10) Gutfleisch, O.; Yan, A.; Müller, K.-H. Large magnetocaloric effect in melt-spun  $\text{LaFe}_{13-x}\text{Si}_x$ . *J. Appl. Phys.* **2005**, *97*, 10M305.
- (11) others,, et al. Mastering hysteresis in magnetocaloric materials. *Philos. Trans. Royal Soc. A* **2016**, *374*, 20150308.
- (12) others,, et al. Hysteresis design of magnetocaloric materials—From basic mechanisms to applications. *Energy Technol.* **2018**, *6*, 1397–1428.
- (13) Gottschall, T.; Skokov, K. P.; Fries, M.; Taubel, A.; Radulov, I.; Scheibel, F.; Benke, D.; Riegg, S.; Gutfleisch, O. Making a cool choice: The materials library of magnetic refrigeration. *Adv. Energy Mater.* **2019**, *9*, 1901322.
- (14) others,, et al. The 2017 magnetism roadmap. *J. Phys. D Appl. Phys.* **2017**, *50*, 363001.
- (15) Mohapatra, J.; Liu, J. P. *Handbook of Magnetic Materials*; Elsevier, 2018; Vol. 27; pp 1–57.
- (16) KuzâĹMin, M.; Skokov, K.; Jian, H.; Radulov, I.; Gutfleisch, O. Towards high-performance permanent magnets without rare earths. *J. Condens. Matter Phys.* **2014**, *26*, 064205.
- (17) Kota, S.; Sokol, M.; Barsoum, M. W. A progress report on the MAB phases: atomically laminated, ternary transition metal borides. *Int. Mater. Rev.* **2019**, 1–30.
- (18) Barsoum, M. W. The  $M_{N+1}AX_N$  phases: A new class of solids: Thermodynamically stable nanolaminates. *Prog. Solid. State Ch.* **2000**, *28*, 201–281.
- (19) Ingason, A. S.; Dahlqvist, M.; Rosén, J. Magnetic MAX phases from theory and experiments: a review. *J. Condens. Matter Phys.* **2016**, *28*, 433003.
- (20) Tan, X.; Chai, P.; Thompson, C. M.; Shatruk, M. Magnetocaloric effect in  $\text{AlFe}_2\text{B}_2$ : toward magnetic refrigerants from earth-abundant elements. *J. Am. Chem. Soc.* **2013**, *135*, 9553–9557.

- (21) Cedervall, J.; Andersson, M. S.; Sarkar, T.; Delczeg-Czirjak, E. K.; Bergqvist, L.; Hansen, T. C.; Beran, P.; Nordblad, P.; Sahlberg, M. Magnetic structure of the magnetocaloric compound  $\text{AlFe}_2\text{B}_2$ . *J. Alloys Compd.* **2016**, *664*, 784–791.
- (22) Barua, R.; Lejeune, B.; Ke, L.; Hadjipanayis, G.; Levin, E. M.; McCallum, R.; Kramer, M.; Lewis, L. Anisotropic magnetocaloric response in  $\text{AlFe}_2\text{B}_2$ . *J. Alloys Compd.* **2018**, *745*, 505–512.
- (23) Chai, P.; Stoian, S. A.; Tan, X.; Dube, P. A.; Shatruk, M. Investigation of magnetic properties and electronic structure of layered-structure borides  $\text{AlT}_2\text{B}_2$  (T= Fe, Mn, Cr) and  $\text{AlFe}_{2-x}\text{Mn}_x\text{B}_2$ . *J. Solid State Chem.* **2015**, *224*, 52–61.
- (24) Kádas, K.; Iuşan, D.; Hellsvik, J.; Cedervall, J.; Berastegui, P.; Sahlberg, M.; Jansson, U.; Eriksson, O.  $\text{AlM}_2\text{B}_2$  (M= Cr, Mn, Fe, Co, Ni): a group of nanolaminated materials. *J. Condens. Matter Phys.* **2017**, *29*, 155402.
- (25) El Boukili, A.; Tahiri, N.; Salmani, E.; Ez-Zahraouy, H.; Hamedoun, M.; Benyoussef, A.; Balli, M.; Mounkachi, O. Magnetocaloric and cooling properties of the intermetallic compound  $\text{AlFe}_2\text{B}_2$  in an AMR cycle system. *Intermetallics* **2019**, *104*, 84–89.
- (26) Ke, L.; Harmon, B. N.; Kramer, M. J. Electronic structure and magnetic properties in  $\text{T}_2\text{AlB}_2$  (T= Fe, Mn, Cr, Co, and Ni) and their alloys. *Phys. Rev. B* **2017**, *95*, 104427.
- (27) Zhang, H.; Dai, F.-z.; Xiang, H.; Zhang, Z.; Zhou, Y. Crystal structure of  $\text{Cr}_4\text{AlB}_4$ : A new MAB phase compound discovered in Cr-Al-B system. *J. Mater. Sci. Technol.* **2019**, *35*, 530–534.
- (28) Khazaei, M.; Wang, J.; Estili, M.; Ranjbar, A.; Suehara, S.; Arai, M.; Esfarjani, K.; Yunoki, S. Novel MAB phases and insights into their exfoliation into 2D MBenes. *Nanoscale* **2019**, *11*, 11305–11314.

- (29) Miao, N.; Wang, J.; Gong, Y.; Wu, J.; Niu, H.; Wang, S.; Li, K.; Oganov, A. R.; Tada, T.; Hosono, H. Computational Prediction of Boron-Based MAX Phases and MXene Derivatives. *Chem. Mater.* **2020**, *32*, 6947–6957.
- (30) Jeitschko, W. Die Kristallstruktur von MoAlB. *Monatsh. Chem.* **1966**, *97*, 1472–1476.
- (31) Jeitschko, W. The crystal structure of Fe<sub>2</sub>AlB<sub>2</sub>. *Acta. Crystallogr. B. Struct. Sci.* **1969**, *25*, 163–165.
- (32) Jung, W.; Schweitzer, K. Die Kristallstrukturen der ternären Boride Al<sub>2</sub>Ru<sub>3</sub>B<sub>2</sub> und Al<sub>3</sub>Ru<sub>4</sub>B<sub>2</sub>. *Z. Kristallogr. Cryst. Mater.* **1986**, *174*, 109–110.
- (33) Chaban, N.; KUZ'MA, I. Ternary systems Cr-Al-B and Mn-Al-B. *Akademiia Nauk SSSR, Izvestiia, Neorganicheskie Materialy* **1973**, *9*, 1908–1911.
- (34) Ade, M.; Hillebrecht, H. Ternary borides Cr<sub>2</sub>AlB<sub>2</sub>, Cr<sub>3</sub>AlB<sub>4</sub>, and Cr<sub>4</sub>AlB<sub>6</sub>: The first members of the series (CrB<sub>2</sub>)<sub>n</sub>CrAl with n= 1, 2, 3 and a unifying concept for ternary borides as MAB-phases. *Inorg. Chem.* **2015**, *54*, 6122–6135.
- (35) Häggström, L.; Wäppling, R.; Ericsson, T.; Andersson, Y.; Rundqvist, S. Mössbauer and X-ray studies of Fe<sub>5</sub>PB<sub>2</sub>. *J. Solid State Chem.* **1975**, *13*, 84–91.
- (36) Hirt, S.; Hilfinger, F.; Hillebrecht, H. Synthesis and crystal structures of the new ternary borides Fe<sub>3</sub>Al<sub>2</sub>B<sub>2</sub> and Ru<sub>9</sub>Al<sub>3</sub>B<sub>8</sub> and the confirmation of Ru<sub>4</sub>Al<sub>3</sub>B<sub>2</sub> and Ru<sub>9</sub>Al<sub>5</sub>B<sub>8-x</sub> (x≈2). *Z. Kristallogr. Cryst. Mater.* **2018**, *233*, 295–307.
- (37) Cedervall, J.; Kontos, S.; Hansen, T. C.; Balmes, O.; Martinez-Casado, F. J.; Matej, Z.; Beran, P.; Svedlindh, P.; Gunnarsson, K.; Sahlberg, M. Magnetostructural transition in Fe<sub>5</sub>SiB<sub>2</sub> observed with neutron diffraction. *J. Solid State Chem.* **2016**, *235*, 113–118.
- (38) McGuire, M. A.; Parker, D. S. Magnetic and structural properties of ferromagnetic Fe<sub>5</sub>PB<sub>2</sub> and Fe<sub>5</sub>SiB<sub>2</sub> and effects of Co and Mn substitutions. *J. Appl. Phys.* **2015**, *118*, 163903.

- (39) Werwiński, M.; Kontos, S.; Gunnarsson, K.; Svedlindh, P.; Cedervall, J.; Höglin, V.; Sahlberg, M.; Edström, A.; Eriksson, O.; Rusz, J. Magnetic properties of  $\text{Fe}_5\text{SiB}_2$  and its alloys with P, S, and Co. *Phys. Rev. B* **2016**, *93*, 174412.
- (40) Lamichhane, T. N.; Taufour, V.; Thimmaiah, S.; Parker, D. S.; Bud'ko, S. L.; Canfield, P. C. A study of the physical properties of single crystalline  $\text{Fe}_5\text{B}_2\text{P}$ . *J. Magn. Magn. Mater.* **2016**, *401*, 525–531.
- (41) Hedlund, D.; Cedervall, J.; Edström, A.; Werwiński, M.; Kontos, S.; Eriksson, O.; Rusz, J.; Svedlindh, P.; Sahlberg, M.; Gunnarsson, K. Magnetic properties of the  $\text{Fe}_5\text{SiB}_2\text{-Fe}_5\text{PB}_2$  system. *Phys. Rev. B* **2017**, *96*, 094433.
- (42) Opahle, I.; Madsen, G. K.; Drautz, R. High throughput density functional investigations of the stability, electronic structure and thermoelectric properties of binary silicides. *Phys. Chem. Chem. Phys.* **2012**, *14*, 16197–16202.
- (43) Opahle, I.; Parma, A.; McEniry, E. J.; Drautz, R.; Madsen, G. K. H. High-throughput study of the structural stability and thermoelectric properties of transition metal silicides. *New J. Phys.* **2013**, *15*, 105010.
- (44) Gao, Q.; Opahle, I.; Gutfleisch, O.; Zhang, H. Designing rare-earth free permanent magnets in heusler alloys via interstitial doping. *Acta Mater.* **2020**, *186*, 355–362.
- (45) Ohmer, D.; Qiang, G.; Opahle, I.; Singh, H. K.; Zhang, H. High-throughput design of  $211 - \text{M}_2\text{AX}$  compounds. *Phys. Rev. Materials* **2019**, *3*, 053803.
- (46) Singh, H. K.; Zhang, Z.; Opahle, I.; Ohmer, D.; Yao, Y.; Zhang, H. High-throughput screening of magnetic antiperovskites. *Chem. Mater.* **2018**, *30*, 6983–6991.
- (47) Saal, J. E.; Kirklin, S.; Aykol, M.; Meredig, B.; Wolverton, C. Materials design and discovery with high-throughput density functional theory: the open quantum materials database (OQMD). *JOM* **2013**, *65*, 1501–1509.

- (48) Kresse, G.; Furthmüller, J. Efficient iterative schemes for ab initio total-energy calculations using a plane-wave basis set. *Phys. Rev. B* **1996**, *54*, 11169.
- (49) Kresse, G.; Joubert, D. From ultrasoft pseudopotentials to the projector augmented-wave method. *Phys. Rev. B* **1999**, *59*, 1758.
- (50) Koepnick, K.; Eschrig, H. Full-potential nonorthogonal local-orbital minimum-basis band-structure scheme. *Phys. Rev. B* **1999**, *59*, 1743.
- (51) Bocarsly, J. D.; Levin, E. E.; Garcia, C. A.; Schwennicke, K.; Wilson, S. D.; Seshadri, R. A simple computational proxy for screening magnetocaloric compounds. *Chem. Mater.* **2017**, *29*, 1613–1622.
- (52) Kirklin, S.; Saal, J. E.; Meredig, B.; Thompson, A.; Doak, J. W.; Aykol, M.; Rühl, S.; Wolverton, C. The Open Quantum Materials Database (OQMD): assessing the accuracy of DFT formation energies. *Npj Comput. Mater.* **2015**, *1*, 15010.
- (53) Werwiński, M.; Edström, A.; Rusz, J.; Hedlund, D.; Gunnarsson, K.; Svedlindh, P.; Cedervall, J.; Sahlberg, M. Magnetocrystalline anisotropy of Fe<sub>5</sub>PB<sub>2</sub> and its alloys with Co and 5d elements: A combined first-principles and experimental study. *Phys. Rev. B* **2018**, *98*, 214431.
- (54) Zhuravlev, I. A.; Antropov, V. P.; Belashchenko, K. D. Spin-fluctuation mechanism of anomalous temperature dependence of magnetocrystalline anisotropy in itinerant magnets. *Phys. Rev. Lett.* **2015**, *115*, 217201.
- (55) Oppeneer, P. Handbook of Magnetic Materials. Vol. 13, Elsevier, Amsterdam **2001**,
- (56) Li, X.-H.; Xing, C.-H.; Cui, H.-L.; Zhang, R.-Z. Elastic and acoustical properties of Cr<sub>3</sub>AlB<sub>4</sub> under pressure. *J. Phys. Chem. Solids* **2019**, *126*, 65–71.
- (57) Zhou, Y.; Xiang, H.; Dai, F.-Z.; Feng, Z. Electrical conductive and damage-tolerant

- nanolaminated MAB phases  $\text{Cr}_2\text{AlB}_2$ ,  $\text{Cr}_3\text{AlB}_4$  and  $\text{Cr}_4\text{AlB}_6$ . *Mater. Res. Lett.* **2017**, *5*, 440–448.
- (58) others., et al. Influence of Cobalt Substitution on the Magnetic Properties of  $\text{Fe}_5\text{PB}_2$ . *Inorg. Chem.* **2018**, *57*, 777–784.
- (59) others., et al. X-ray investigations of the ternary system Fe-P-B. Some features of the systems Cr-P-B, Mn-P-B, Co-P-B and Ni-P-B. *Acta Chem. Scand.* **1962**, *16*, 1–19.
- (60) Bormio-Nunes, C.; Nunes, C. A.; Coelho, A. A.; Faria, M. I. S. T.; Suzuki, P. A.; Coelho, G. C. Magnetization studies of binary and ternary Co-rich phases of the Co–Si–B system. *J. Alloys Compd.* **2010**, *508*, 5–8.
- (61) Baurecht, H.; Boller, H.; Nowotny, H. Röntgenographische Untersuchungen in den Dreistoffen Cr-P-C, Cr-As-C und Cr-P-B. *Monatsh. Chem.* **1971**, *102*, 373–384.
- (62) Guy, C.; Uraz, A. The chromium-boron system. *J. Less Common Met.* **1976**, *48*, 199–203.
- (63) Xie, Z.; Geng, D.; Zhang, Z. Reversible room-temperature magnetocaloric effect in  $\text{Mn}_5\text{PB}_2$ . *Appl. Phys. Lett.* **2010**, *97*, 202504.
- (64) Wang, X.; Xiao, R.; Li, H.; Chen, L. Oxysulfide  $\text{LiAlSO}$ : a lithium superionic conductor from first principles. *Phys. Rev. Lett.* **2017**, *118*, 195901.
- (65) Jain, A.; Ong, S. P.; Hautier, G.; Chen, W.; Richards, W. D.; Dacek, S.; Cholia, S.; Gunter, D.; Skinner, D.; Ceder, G.; Persson, K. a. The Materials Project: A materials genome approach to accelerating materials innovation. *APL Mater.* **2013**, *1*, 011002.
- (66) Opahle, I.; Singh, H. K.; Zemen, J.; Gutfleisch, O.; Zhang, H. Effect of N, C and B interstitials on the structural and magnetic properties of alloys with  $\text{Cu}_3\text{Au}$ -structure. *arXiv preprint arXiv:2001.00959* **2020**,

- (67) Potashnikov, D.; Caspi, E.; Pesach, A.; Hoser, A.; Kota, S.; Verger, L.; Barsoum, M.; Felner, I.; Keren, A.; Rivin, O. Magnetic ordering in the nano-laminar ternary  $\text{Mn}_2\text{AlB}_2$  using neutron and X-ray diffraction. *J. Magn. Magn. Mater.* **2019**, *471*, 468–474.
- (68) Cedervall, J.; Andersson, M. S.; Iuşan, D.; Delczeg-Czirjak, E. K.; Jansson, U.; Nordblad, P.; Sahlberg, M. Magnetic and mechanical effects of Mn substitutions in  $\text{AlFe}_2\text{B}_2$ . *J. Magn. Magn. Mater.* **2019**, *482*, 54–60.
- (69) Mouhat, F.; Coudert, F.-X. Necessary and sufficient elastic stability conditions in various crystal systems. *Phys. Rev. B* **2014**, *90*, 224104.
- (70) Bai, Y.; Qi, X.; He, X.; Sun, D.; Kong, F.; Zheng, Y.; Wang, R.; Duff, A. I. Phase stability and weak metallic bonding within ternary-layered borides  $\text{CrAlB}$ ,  $\text{Cr}_2\text{AlB}_2$ ,  $\text{Cr}_3\text{AlB}_4$ , and  $\text{Cr}_4\text{AlB}_6$ . *J. Am. Chem. Soc.* **2019**, *102*, 3715–3727.
- (71) Mizutani, U. Hume-Rothery rules for structurally complex alloy phases. *MRS Bull.* **2012**, *37*, 169–169.
- (72) Zhang, Y.; Mao, Z.; Han, Q.; Li, Y.; Li, M.; Du, S.; Chai, Z.; Huang, Q. The role of Hume-Rothery’s rules play in the MAX phases formability. *Materialia* **2020**, *12*, 100810.
- (73) Maintz, S.; Deringer, V. L.; Tchougréeff, A. L.; Dronskowski, R. LOBSTER: A tool to extract chemical bonding from plane-wave based DFT. *J. Comput. Chem.* **2016**, *37*, 1030–1035.
- (74) Bruno, P. Tight-binding approach to the orbital magnetic moment and magnetocrystalline anisotropy of transition-metal monolayers. *Phys. Rev. B* **1989**, *39*, 865.
- (75) Halleman, B.; Wollants, P.; Roos, J. Thermodynamic reassessment and calculation of the Fe-B phase diagram. *Z. Metallkd.* **1994**, *85*, 676–682.

- (76) Thakur, J.; Rani, P.; Tomar, M.; Gupta, V.; Kashyap, M. K. Enhancement of magnetic anisotropy of Fe<sub>5</sub>PB<sub>2</sub> with W substitution: ab-initio study. *AIP Conf. Proc.* 2019; p 020012.
- (77) Antropov, V.; Ke, L.; Åberg, D. Constituents of magnetic anisotropy and a screening of spin-orbit coupling in solids. *Solid State Commun.* **2014**, *194*, 35–38.
- (78) Richter, M. Band structure theory of magnetism in 3d-4f compounds. *J. Phys. D Appl. Phys.* **1998**, *31*, 1017.
- (79) Daalderop, G.; Kelly, P.; Schuurmans, M. Magnetocrystalline anisotropy and orbital moments in transition-metal compounds. *Phys. Rev. B* **1991**, *44*, 12054.
- (80) Arora, P.; Chattopadhyay, M.; Roy, S. Magnetocaloric effect in MnSi. *Appl. Phys. Lett.* **2007**, *91*, 062508.
- (81) Yu, M.; Lewis, L.; Moodenbaugh, A. Large magnetic entropy change in the metallic antiperovskite Mn<sub>3</sub>GaC. *J. Appl. Phys.* **2003**, *93*, 10128–10130.

# Graphical TOC Entry

